FULL PAPER

Study of the synthesis of C:H coating by PECVD for protecting Mg-based nano-objects

Hui Liang[1,2] | Adriano Panepinto[2] | Loic Prince[3] | Marjorie Olivier[3,4] |
Damien Cossement[4] | Etienne Bousser[5] | Xi Geng[1] | Wenjiang Li[1,6] |
Minfang Chen[1,6] | Rony Snyders[2,4] | Damien Thiry[2]

[1]School of Materials Science and
Engineering, Tianjin University of
Technology, Tianjin, China

[2]Chimie des Interactions Plasma-Surface,
University of Mons, Mons, Belgium

[3]Materials Science Department, University
of Mons, Mons, Belgium

[4]Materia Nova Research Center, Mons,
Belgium

[5]Functional Coating and Surface
Engineering Laboratory, Ecole
Polytechnique de Montréal, Montréal,
Canada

[6]Key Laboratory of Display Materials and
Photoelectric Device (Ministry of
Education), Tianjin, China

Correspondence
Damien Thiry, Chimie des Interactions
Plasma-Surface, University of Mons, 20
Place du Parc, B 7000 Mons, Belgium.
Email: damien.thiry@umons.ac.be

Abstract

In the context of protecting Mg-based nano-objects for potential hydrogen
storage applications, the potential of C:H layer as a barrier polymer material
deposited by the plasma-enhanced chemical vapor deposition process is
examined. Corrosion tests reveal (a) good barrier properties of the C:H layer
and (b) suggest an increase in
the internal stress with the
power dissipated in the plas-
ma. The latter is attributed to
an increase in the cross-
linking density of the coat-
ings accompanied by an in-
crease in the stiffness as
shown by nanoindentation
measurements. Finally, for a
given set of plasma para-
meters, Mg-based nanowires
were successfully enrobed by
the C:H coatings as evi-
denced by scanning electron
microscopy measurements.

KEYWORDS

C:H plasma polymer films, corrosion barrier, hydrogen storage, Mg nanowires

1 | INTRODUCTION

Nowadays, hydrogen is considered as a promising al-
ternative energy carrier that can potentially facilitate
the transition from fossil to renewable fuels because
of its prominent advantages such as high energy
density, great variety of potential sources, lightweight,

and low environmental impact.[1–6] Nevertheless,
important issues (e.g., hydrogen production, trans-
port, storage, etc.) have to be addressed before the use
of hydrogen as an energy source becomes industrially
and economically viable. Today, specifically in the
automotive industry, one of the main obstacles is
clearly the lack of efficient hydrogen storage requiring

the development of effective methods for hydrogen compression.[4]

In this context, the use of hydride materials (where hydrogen is chemically bonded to a metal), especially MgH_2-based one, able to store important quantities of hydrogen has emerged.[2–7] For an efficient hydrogen storage process, the ability for the Mg-based material to form a stable thermodynamic state with hydrogen but weakly enough to release it on demand with a small temperature rise is mandatory.[1] This can be achieved by reducing the size of the Mg-based material down to nanoscale.[3,8] In addition, protecting the nano-objects to avoid the oxidation of Mg giving rise to the formation of MgO or $Mg(OH)_2$ and thus limiting the diffusion of hydrogen in the material, is also crucial.[1] Based on these considerations, it has been reported that embedding nanosized Mg-based objects in a polymeric matrix acting as protecting material against the oxidation of the nanostructures appears as a very promising approach.[1,3,9] Besides offering protection against oxidation, the polymeric matrix has also to fulfill additional requirements. For instance, when forming the MgH_2 phase from metallic Mg, a volume expansion of about 33% takes place as a consequence of hydrogen uptake.[1,7] Therefore, the mechanical flexibility of the polymer is also an important criterion. Furthermore, considering the industrial perspective, the current environmental context makes more and more urgent the development of green technologies for material synthesis.

In this context, plasma-based technologies combining several prominent advantages (i.e., environmentally friendly, time-efficient, industrially scalable) attract considerable attention for material synthesis.[10–12] The main advantage is likely the versatility of these surface engineering processes enabling to modulate in a wide range the physicochemical properties of the synthesized material by a clever choice of the process parameters. On this basis, in this study, we propose to evaluate the potential of a C:H plasma polymer film (PPF) deposited by plasma-enhanced chemical vapor deposition (PECVD) from ethylene precursor as a protective coating for Mg-based nano-objects. The choice of this material is motivated by previous works revealing its efficiency as a protecting layer.[13,14] Our research strategy includes first, the investigation of the deposition kinetics and the physicochemical properties (i.e., barrier properties, mechanical properties, cross-linking degree, carbon hybridization, chemical composition) of the C:H layer (using silicon or aluminum as substrates) as a function of the load of energy in the plasma. Then, for a selected synthesis condition, the

covering of Mg-based nanowires fabricated by magnetron sputtering operating in glancing angle geometry as recently reported in our group[15] is carried out. The conformality of the C:H layer on the nano-objects is examined by electronic microscopy.

2 | EXPERIMENTAL PART

All experiments were carried out in a cylindrical stainless steel chamber (height: 60 cm, diameter: 42 cm). The chamber was evacuated by a turbomolecular pump (Edwards nEXT400D 160 W; Burgess Hill, UK), down to a residual pressure of 10^{-6} Pa. A magnetron cathode was installed at the top of the chamber and the substrate was located at a distance of 80 mm. A 2-inch in diameter and 0.25-inch thick Mg target (99.99% purity) was used. Conductive silicon wafers (100) or polished aluminum were used as substrates and rinsed with ultrapure water before deposition.

The synthesis of the Mg-based nanowires, which will be further covered by the C:H layers is performed by sputtering the target in DC mode using an Advanced Energy MDK 1.5K power supply (with a power kept constant at 50 W) in an argon atmosphere using a flow of 12 sccm. The working pressure was 0.13 Pa. To induce the formation of the nanowires, the substrate was tilted during the synthesis at a value of 87°. More details can be found in Liang et al.[15]

For the synthesis of the C:H coating, the working pressure and the ethylene flow rate were fixed to 13 Pa and 15 sccm, respectively. The Mg target was sputtered using a radiofrequency (RF) power supply (Advanced Energy) operating at 13.56 MHz and connected to the cathode through a matching network. The influence of the RF power applied to the cathode (P_{RF}) was studied in the range 20–100 W. In our experimental window, the self-bias of the target evolves from −100 to −312 V with P_{RF}. In all the experiments, the substrate is kept at the floating potential.

The thickness of the C:H coatings is measured using a Sloan Dektak 3030ST mechanical profilometer. For these experiments, a step was generated using a mask.

Raman spectra measurements (400–2,000 cm^{-1}) were carried out in a Bruker Senterra spectrometer equipped with a charge-coupled device detector and a He–Ne laser (532 nm) at 10 mW.

The films were also investigated by Fourier-transform infrared spectroscopy (FTIR) using an Excalibur FTS 3000 FTIR spectrometer from Bio-RAD. Spectra from 400 to 4,000 cm^{-1} were recorded with a resolution of 4 cm^{-1} and averaged over 2,048 scans to accumulate a good signal-to-noise ratio. For these experiments, the C:H

coatings (thickness of 500 nm) are deposited on KBr pastille.

The morphological characterizations were carried out using a field emission gun scanning electron microscope (FEG-SEM; Hitachi SU8020; Ri Li, Japan).

To evaluate the cross-linking density of the C:H layers, static time-of-flight secondary ion mass spectrometry (ToF-SIMS) measurements were acquired using a ToF-SIMS IV instrument from IONTOF GmbH. The as-deposited films are exposed a few minutes in the air before their introduction in the instrument. A 10-keV Ar^+ ion beam at a current of 0.5 pA rastered over a scan area of $200 \times 200 \, \mu m^2$ during 150 s. The positive spectra were analyzed by the principal component analysis (PCA) method using the SIMCA-P13 software supplied by Umetrics, Sweden. Before multivariate analysis, each spectrum was normalized to total ion count number, mean-centered, and scaled. More details about the PCA treatment can be found elsewhere.[16]

The hardness and modulus of the films were measured by depth-sensing indentation using a Bruker/Hysitron Triboindenter with a diamond Berkovich pyramidal tip. Before testing, the tip geometry and system compliance were calibrated using a fused silica standard and, before each indentation, the thermal drift of the system was measured and the displacement data corrected. A trapezoidal load function was used for these indentations with 5-s loading and unloading segments and a 2-s hold in between. The load–displacement curves of each indentation were analyzed using the Oliver–Pharr methodology.[17] To evaluate the mechanical properties as a function of penetration depth, each film was indented by three 5×5 indentation arrays with a spacing of $5 \, \mu m$ between indentations. Within each array the indentation load was decreased incrementally from a maximum of 9 mN for the first indentation down to 0.1 mN for the last. Finally, to extract the hardness and modulus of the films without the contribution from the substrate, we followed the methodology proposed in the ISO standard 14577-4.[18] The sample mechanical properties where thus averaged from those obtained from the three indentation arrays per sample, with the standard deviation representing the error.

The study of the corrosion resistance of the C:H coatings is achieved using electrochemical impedance spectroscopy (EIS). For these measurements, the C:H coatings are deposited on aluminum substrates (1050 AA, 20×20 mm) which, before the synthesis, were degreased using acetone and methanol and mechanically polished up to 2,200 grade to remove the superficial oxide and the impurity layer. EIS measurements were performed in a three-electrode cell in a frequency range from 100 kHz to 100 mHz using an amplitude signal of 5 mV.

The impedance spectra were performed using a Parstat Model 2273 controlled by PowerSuite® software. An Ag/AgCl/KCl saturated reference electrode, a platinum counter-electrode, and a working electrode made of the studied sample were employed. The sample area exposed to 0.1 M NaCl electrolyte solution was $1 \, cm^2$. During the immersion period, the volume of the solution was maintained at 20 ml. To minimize external electromagnetic interferences on the measurements, the electrochemical cell was placed in a Faraday cage.

3 | RESULTS AND DISCUSSION

In the first attempt, the deposition kinetics of the C:H layer as a function of the injected power is examined (Figure 1). The deposition rate increases from ~5 to ~22 nm/min for P_{RF} evolving from 20 to 100 W. Giving our specific experimental configuration, the growth of the layer could, in principle, come from two distinct contributions: (a) the condensation of the sputtered particles from the magnesium target and (b) the adsorption of reactive species (i.e., ions and mainly radicals) resulting from the precursor dissociation.[19] Nevertheless, it has been reported that for pure carbon-based precursor discharge (i.e., no Ar), the growth of the layer can mainly be ascribed to the chemisorption of the film-forming species formed in the gas phase.[20] Thus, the process can be considered to operate in a pure PECVD mode. This is further supported by the absence of Mg lines in the X-ray photoelectron (XPS) spectra (Figure 2).

Considering that only the PECVD process contributes to the film growth, the increase in the deposition rate with the load of energy is ascribed to an increase in the electron density. As a consequence, a higher concentration
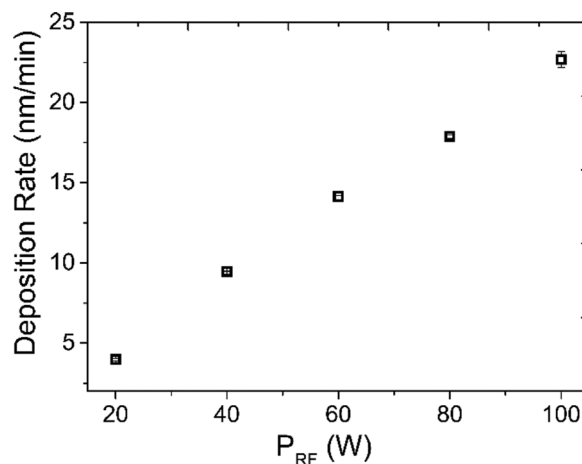

FIGURE 1 Evolution of the deposition rate for the synthesis of the C:H coating as a function of P_{RF}
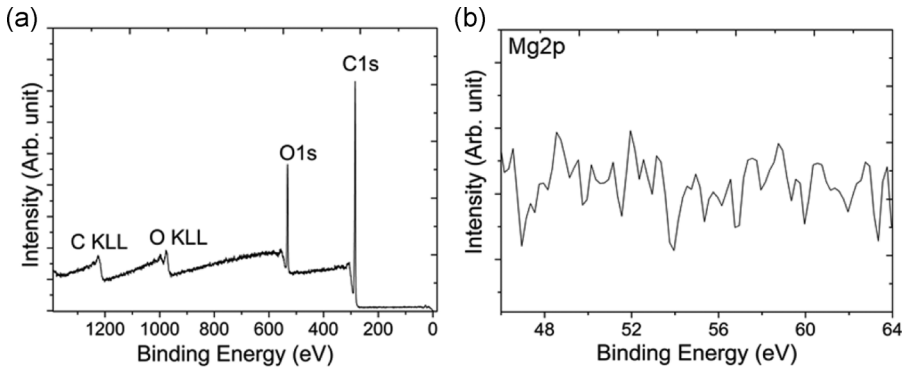
FIGURE 2 (a) Typical X-ray photoelectron spectroscopy survey and (b) high-resolution Mg 2p photoelectron peak of an as-deposited C:H layer synthesized for $P_{RF} = 20$ W

of film-forming species (i.e., mainly radicals) is produced through collisional processes giving rise to an increase in the deposition rate.[21,22]

To evaluate the barrier properties of the coatings, corrosion tests have been performed using polished Al substrates. As the corrosion of Al occurs through O_2 and H_2O diffusion, such an approach can be used to characterize the barrier properties of the deposited PPF against O_2. This is achieved by EIS measurements carried out on coated and uncoated samples. This technique does not only gives information about the barrier properties of the PPF but also about the potential corrosion processes at the metal–coating interface. The evolutions of the impedance modulus and phase diagrams as a function of the immersion time (i.e., after 3 and 7 days), the so-called Bode diagram, in 0.1 M NaCl solution for an uncoated polished 1050 aluminum alloys samples are shown in Figures 3a and 3b, respectively.

The analysis of the Bode diagram of the uncoated Al substrate reveals stable electrochemical behavior during the full experiment period. This phenomenon is explained by the protective alumina layer naturally present on the surface of the metallic substrate as well as the low surface roughness, which limits galvanic corrosion phenomena. The low frequency (100 mHz) modulus, representative to the total barrier resistance of the system, is about 10^6 Ω·cm^2. Therefore, an improvement of the corrosion protection will be indicated by an increase in the low-frequency modulus.[24] Moreover, on the Bode phase diagrams, the behavior at low and medium frequencies after 7 days of immersion corresponds to a capacitive behavior that can be associated with the capacitance of the alumina layer. [25,26]

As it can be seen in Figure 4, when a 200 nm thick C:H layer ($P_{RF} = 20$ W) is grown on the Al substrate, a significant improvement in the corrosion properties is observed. Namely, the low-frequency modulus (100 mHz) is increased by one order of magnitude (as compared with the uncoated Al substrate) to reach values around 10^7 Ω·cm^2 after 7 days of immersion. The enhancement of corrosion protection is obviously attributed to the presence of a dense amorphous cross-linked C:H coating film providing an extra barrier against penetration of aggressive species (i.e., O_2, H_2O, Cl^-). Moreover, the time constant could be associated with the response of the film capacitance and resistance, as it presents a phase angle value (from $-80°$ to $-70°$) characteristic of such capacitive behavior.
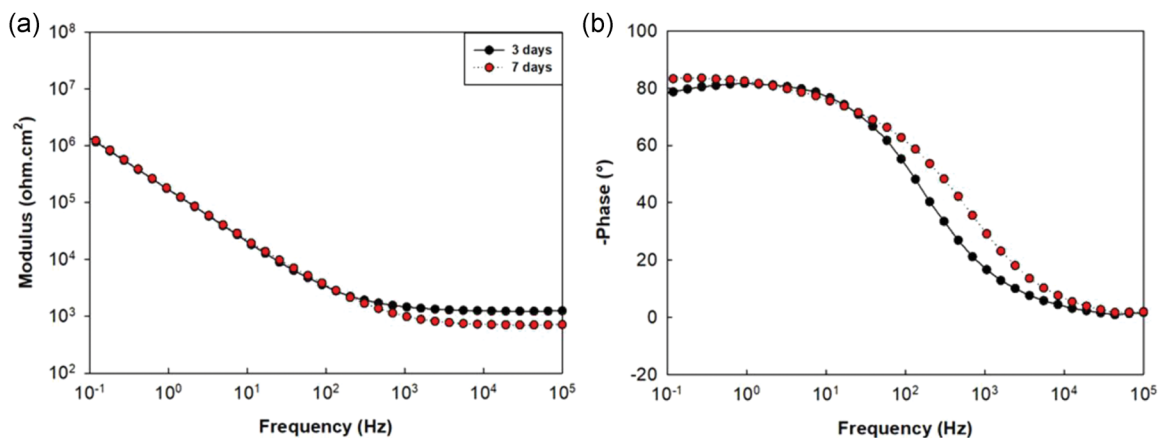

FIGURE 3 Bode diagrams in (a) modulus and (b) phase of an uncoated Al substrate for different immersion times in 0.1 M NaCl
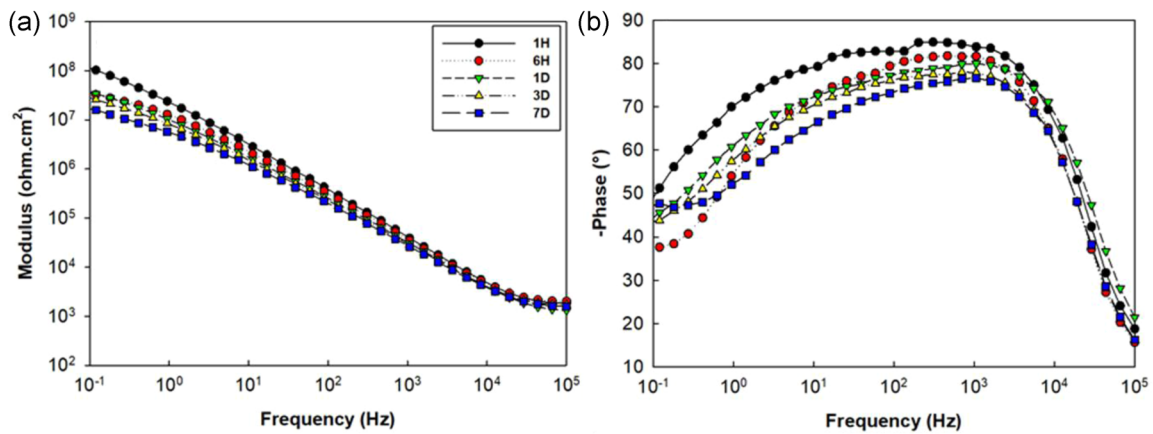
FIGURE 4 Bode diagrams in (a) modulus and (b) phase as a function of the immersion time in 0.1 M NaCl for an Al substrate covered by a C:H layer deposited for $P_{RF} = 20W$

To compare the corrosion barrier efficiency of the PPF layer as a function of their growth conditions, a 200 nm thick C:H layer ($P_{RF} = 60$ W) is deposited on the Al substrate. For this PPF growth conditions, the Bode diagrams (Figure 5) are composed of at least two time constants: the time constant at a lower frequency, which can be associated with the native alumina present on the aluminum substrate with its capacitive behavior identifiable in the middle-frequency range on the Bode diagrams. The second time constant at higher frequency (10^4 Hz) is related to the contribution of the resistance and capacitance of the PPF layer. This time constant is strongly reduced compared with its homologous obtained for $P_{RF} = 20$ W. After 7 days, the relative time constant disappears and only a resistive behavior can be observed at high frequency. For the sake of completeness, a similar experiment has been carried out for a PPF deposited for $P_{RF} = 100$ W, revealing an identical behavior (see Figure S1). This could be attributed to the cracking/delamination of the layer when immersed in an

aqueous solution due to excessive internal stress. Indeed, it has been reported that C:H thin films synthesized by PECVD often present high internal compressive stress, which could potentially result in the coating failure in solution.[27,28] Based on these considerations, it is proposed here that increasing P_{RF} results in the formation of C:H PPF films with higher residual stress, in line with the literature.[29]

As aforementioned in Section 1, considering hydrogen storage applications, during the "hydrogenation" reaction, a volume expansion of ~33% occurs.[1,7] If containing too high internal stress, the volume expansion that the metal undergoes during the adsorption cycle might result in the formation of cracks in the polymer network offering preferential pathways for the oxidation of the Mg-based nano-objects. The internal stress of the polymeric matrix therefore also represents an important factor. In contrast, the availability for the polymeric matrix to mechanically accommodate during the
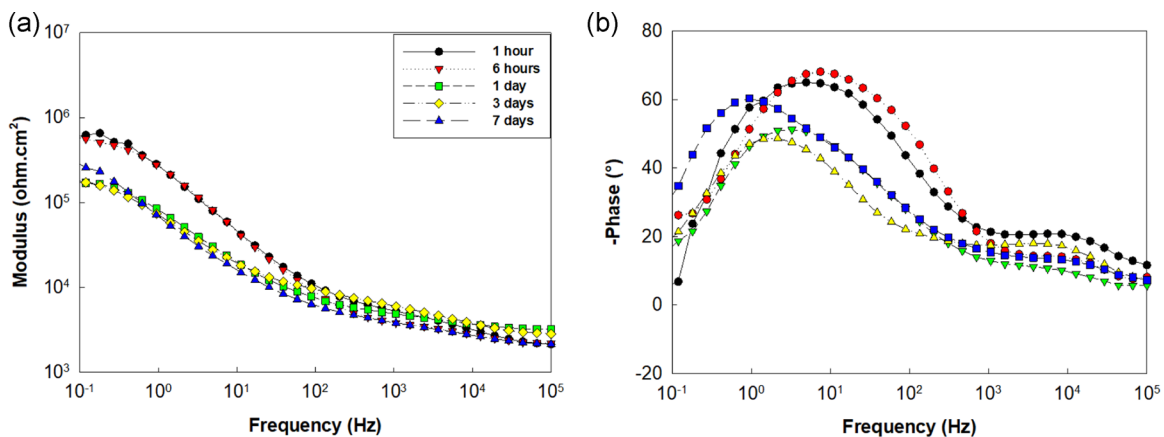

FIGURE 5 Bode diagrams in (a) modulus and (b) phase of an Al substrate covered by a C:H layer synthesized for $P_{RF} = 60$ W versus immersion times in 0.1 M NaCl

expansion also strongly depends on its mechanical properties. Therefore, nanoindentation measurements have been carried out to evaluate the hardness and Young's modulus of the C:H layers.

As shown in Figure 6, both Young's modulus (i.e., from ~5 to ~12 GPa) and hardness (i.e., from ~1 to ~1.8 GPa) increase with P_{RF}. The control over the stiffness of the C:H layer would enable to modulate the flexibility of the PPF coating, which is important as already mentioned regarding the adsorption/desorption cycle. Referring to the range of hardness measured in this study, these C:H layers can be classified as polymer-like hydrogenated films and do not belong to the category of "diamond-like carbon"-based material exhibiting higher hardness.[30–33]

The evolution of the stiffness as well as the internal stress of the coatings regarding the load of energy is expected to result from variation in the chemical composition (e.g., sp^3 vs. sp^2 carbon bonding configuration) and/or cross-linking density.[28,34] Therefore, to gain more information, Raman/FTIR spectroscopies and ToF-SIMS measurements are carried out to evaluate the chemical composition as well as the cross-linking degree of the C:H layers as a function of P_{RF}, respectively.

Figure 7 represents the Raman spectra of the C:H coatings as a function of P_{RF}. The absence of sp^2 signature characterized by the nondetection of the associated G (1,580 cm^{-1}) and D (1,350 cm^{-1}) peaks indicates the formation in our experimental window of a hydrogenated polymer-like layer mainly composed of sp^3 hybridized carbon validating our previous observation regarding the range of hardness measured.[35] These conclusions are further confirmed by FTIR measurements (Figure 8) also revealing the absence of sp^2 signature in the spectra. Indeed, mainly CH$_3$ (i.e., antisymmetric stretching at 2,957 cm^{-1}, antisymmetric bending at 1,454–1,456 cm^{-1} and symmetric bending at 1,375–1,381 cm^{-1}) and CH$_2$ (i.e., antisymmetric stretching at

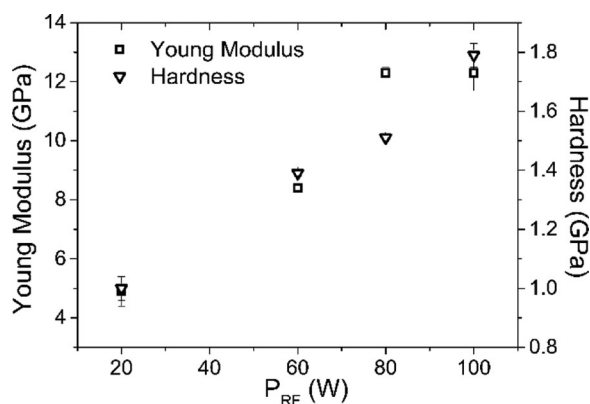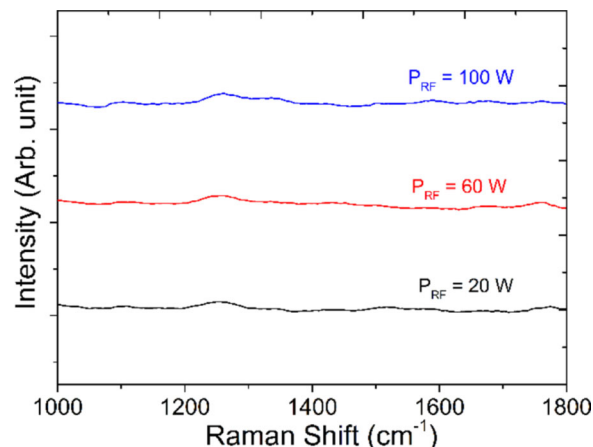**FIGURE 7** Raman spectra of the C:H coatings as a function of P_{RF}

2,932–2,939 cm^{-1}, symmetric stretching at 2,872–2,879 cm^{-1}, and symmetric bending at 1,454–1,456 cm^{-1}) vibration modes are identified.[36] For the sake of completeness, the presence of oxygen-based functionalities (i.e., OH stretching at 3,443–3,470 cm^{-1}, C=O stretching at 1,715–1,718 cm^{-1}) is ascribed to the post-oxidation of the layers in the air during the storage of the samples before their analysis.[37]

Regarding the ToF-SIMS analysis, as mass spectra of organic-based coatings often contain dozen of peaks, a statistical treatment using the PCA method is employed to address this issue of data abundance.[38,39] This strategy allows to extract the essential information concerning the variation in surface chemistry depending on the process parameters. More details about this data treatment can be found in the review of Cossement et al.[16] Figure 9 shows the "score" plot extracted from the PCA treatment of our ToF-SIMS spectra in which the data are
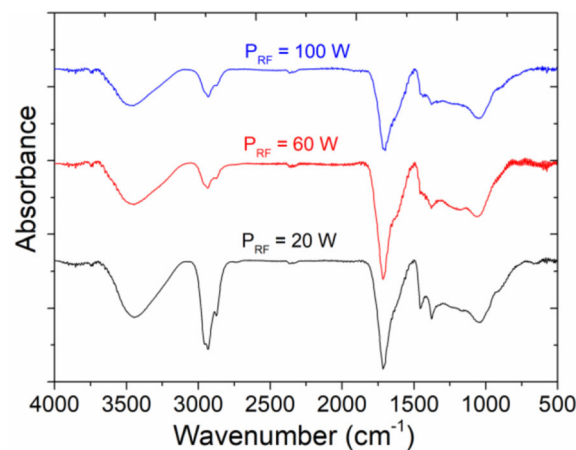

FIGURE 6 Evolution of Young's modulus and the hardness of the C:H layer as a function of P_{RF}

FIGURE 8 Fourier-transform infrared spectra of the C:H coatings as a function of P_{RF}
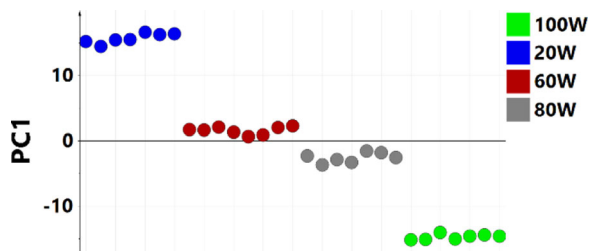
FIGURE 9 Score plot showing sample discrimination as a result of principal component analysis processing of the time-of-flight secondary ion mass spectrometry data

positioned according to their surface fragmentation pattern. The larger is the distance between the points, the larger is the difference between the corresponding ToF-SIMS mass spectra, thus revealing variation in terms of surface chemistry. Regarding P_{RF}, the samples are well discriminated along the axis, namely the principal component, that is, PC1.

The PCA model also gives the most influential peaks in the PC1 model, responsible for sample discrimination in the score plot. Indeed, a positive or negative loading coefficient (giving the statistical weight) is associated with each m/z signal. The higher the absolute value of the loading coefficient, the higher is the intensity variation of the corresponding peak from sample to sample. The C:H layers synthesized for $P_{RF} = 80$ and 100 W are characterized by negative loadings as they are positioned in the negative part of the score plot when considering the PC1 axis while the reverse situation is observed for samples synthesized for $P_{RF} = 20$ and 60 W. To gain information about the cross-linking degree, the average chemical composition of the fragments was calculated for each loading category (i.e., negative and positive) following a method described elsewhere.[16,38,39] Considering the most statistically important peaks (i.e., peaks having a statistical weight >90%) based on the data depicted in Figure S2, the carbon and hydrogen atoms of each influential associated signal is summed up and then divided by the numbers of considered peaks. In our case, the calculated average fragments are $C_6H_{4.5}^+$ and $C_{9.8}H_{9.5}^+$ for negative (i.e., $P_{RF} = 80$ and 100 W) and positive (i.e., for $P_{RF} = 20$ and 60 W) loadings, respectively. For each fragment, the C/H ratio giving direct information about the cross-linking degree is examined. An increase in P_{RF} gives rise to a higher C/H ratio (1.33 vs. 1.03) indicating an increase in the cross-linking degree of the C:H layers with the load of energy.

It can, therefore, be concluded from the chemical and structural characterization of the samples that the C:H layers consist of a hydrogenated polymer-like thin film, mainly formed by sp^3 carbon with a tunable cross-linking degree, impacting the stiffness as well as the internal stress. To explain this behavior, let us consider the overall growth mechanism. Briefly, reactive species including ions and mainly radicals are generated in the plasma through electron-impact-induced dissociation reactions of the precursor. Then, the adsorption of the formed species at the growing film interface gives rise to the growth of the layer. As evidenced by the increase in the deposition rate, the flux of radicals reaching the interface likely increases with P_{RF} resulting in more recombination reactions between radicals at the surface and in turn a more cross-linked network. Simultaneously, energy is also continuously provided at the growing film interface through ionic bombardment, which, among others, could create surface dangling bonds mainly through C–H bond breaking.[31] As previously reported,[40] increasing P_{RF} results in an increase in the ion flux toward the interface giving rise to more surface recombination of carbon-centered adjacent radicals, thus contributing to an increased cross-linking density of the C:H coatings. This could also induce an increase in the internal stress as the latter is also associated with the densification of the polymeric layer.[41]

Finally, in view of the fabrication of Mg/C:H nanocomposite material for potential hydrogen storage applications, the C:H layer (for $P_{RF} = 20$ W) is deposited on Mg-based nanosculpted films. For these experiments, as a first step, the Mg target is sputtered in pure Ar atmosphere and the substrate is tilted at a value of 87° resulting in the formation of Mg-based nanowires with a length of ~700 ± 100 nm and a width of ~200 ± 20 nm (Figure 10a). This synthesis has been previously reported in detail.[15] In the second step, the C:H coating is deposited on the Mg film in the same reactor varying the deposition time without any venting to avoid the oxidation of the nanowires before their covering.

For a deposition time of 9 min, the top of the nanowires (along a length of about 200 nm) is covered by the C:H layer (Figure 10b) as testified by the increase in the dimension of the columns (i.e., from ~200 ± 20 to ~300 ± 30 nm). The preferential deposition on the top of the column might be tentatively explained by a nonuniform ionic flux over the length of the nanowires. Indeed, assuming a higher ionic flux at the top of the nanowires, it would cause the formation of higher surface reactive sites suitable for the subsequent chemisorption of film-forming species. This would lead to a higher deposition rate at the top of the nano-objects explaining the obtained morphology. Increasing the deposition time to 20 min results in the covering of the entire nanowires with a thickness of the polymer-like layer decreasing from the top to the bottom (Figure 10c). For higher deposition duration, the covered nanowires start to touch resulting
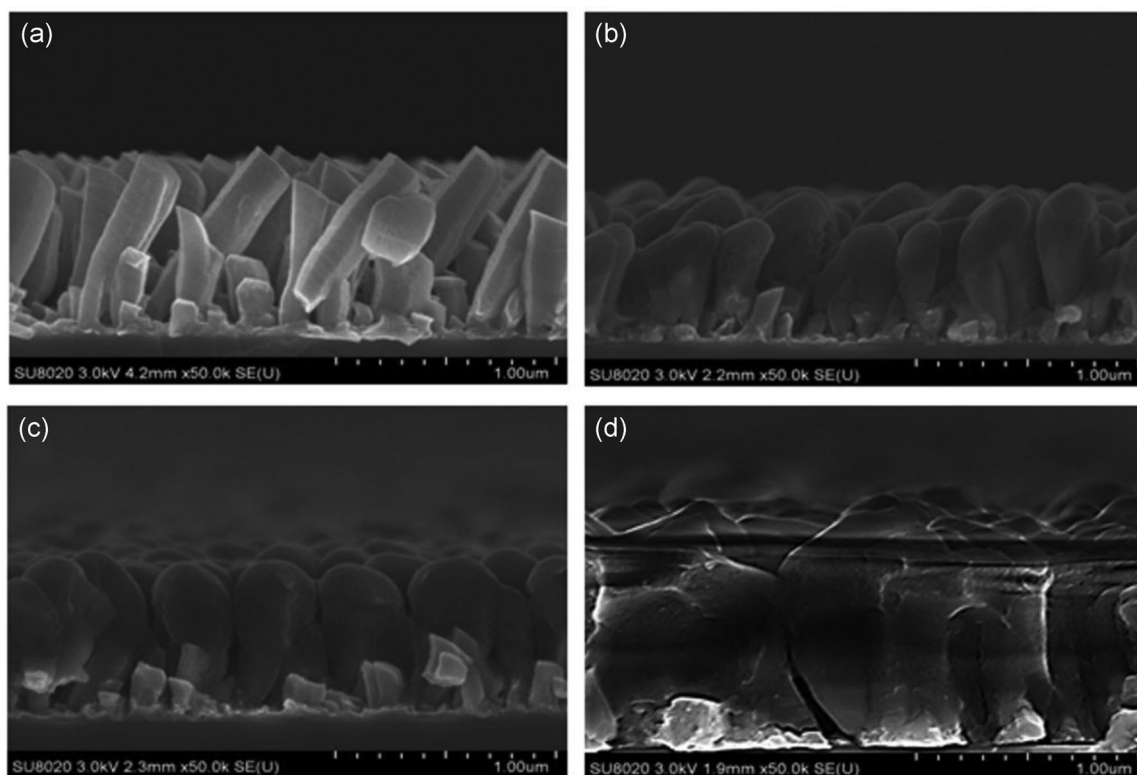
FIGURE 10 Series of cross-section scanning electron micrographs showing the different morphologies obtained after the deposition of the C:H layer on Mg-based nanowires for (a) 0 min, (b) 9 min, (c) 20 min, and (d) 40 min

in the formation of a dense carbon-based layer embedding Mg-based nanocolumns (Figure 10d).

From these data, it appears that, in our experimental conditions, a minimum duration of ~10 min is necessary to obtain a reliable covering of the Mg nanostructure that would allow to protect the coating from oxidation, which is promising for the foreseen application.

4 | CONCLUSIONS

In this study, the deposition kinetics and the physico-chemical properties of C:H coatings synthesized by PECVD are studied in view of the use of the material as a protecting layer for Mg-based nano-objects.

The thorough characterization of the carbon-based layer revealed that the material is mainly formed by a hydrogenated polymer-like skeleton with carbon in sp^3 hybridization. The cross-linking density of the polymer network was found to increase with the load of energy in the plasma. This evolution is accompanied by an increase in the stiffness as well as in the internal stress of the C:H layer as suggested by corrosion tests, which also reveals good barrier properties of the coating. The availability to tune all these features represents a prominent advantage as they are crucial to develop a suitable polymer-based

corrosion barrier of Mg-based nanostructures in the context of hydrogen storage applications. Furthermore, morphological characterizations revealed the efficiency of our method to enrobe Mg-based nanowires, which would offer an ideal protection against oxidation, also crucial for efficiently adsorbing/desorbing hydrogen. The potential of our material for this applicative purpose will be discussed in a forthcoming work.

ORCID
Adriano Panepinto http://orcid.org/0000-0002-5133-5834
Damien Thiry http://orcid.org/0000-0001-6703-1512

REFERENCES
[1] K.-J. Jeon, H. R. Moon, A. M. Ruminski, B. Jiang, C. Kisielowski, R. Bardhan, J. J. Urban, *Nat. Mater.* **2011**, *10*, 286.
[2] A. Züttel, A. Remhof, A. Borgschulte, O. Friedrichs, *Philos. Trans. R. Soc., A* **2010**, *368*, 3329.
[3] Y. Jia, C. Sun, S. Shen, J. Zou, S. S. Mao, X. Yao, *Renewable Sustainable Energy Rev.* **2015**, *44*, 289.

[4] I. Jain, C. Lal, A. Jain, *Int. J. Hydrogen Energy* **2010**, *35*, 5133.

[5] S. E. Hosseini, M. A. Wahid, *Renewable Sustainable Energy Rev.* **2016**, *57*, 850.

[6] K. Mazloomi, C. Gomes, *Renewable Sustainable Energy Rev.* **2012**, *16*, 3024.

[7] C. Zlotea, J. Lu, Y. Andersson, *J. Alloys Compd.* **2006**, *426*, 357.

[8] S. Cheung, W. Deng, A. Van Duin, *J. Phys. Chem. A* **2006**, *109*, 851.

[9] R. W. Wagemans, J. H. Van Lenthe, P. E. De Jongh, A. J. Van Dillen, K. P. De Jong, *J. Am. Chem. Soc.* **2005**, *127*, 16675.

[10] D. Thiry, S. Konstantinidis, J. Cornil, R. Snyders, *Thin Solid Films* **2016**, *606*, 19.

[11] D. Thiry, F. Reniers, R. Snyders *Surface Modification of Polymers: Methods and Applications* (Eds: J. Pinson, D. Thiry), Wiley, Weinheim **2019**, p. 67.

[12] J. Friedrich, *Plasma Processes Polym.* **2011**, *8*, 783.

[13] S. Vasquez-Borucki, W. Jacob, C. A. Achete, *Diamond Relat. Mater.* **2000**, *9*, 1971.

[14] A. Ogino, M. Nagatsu, *Thin Solid Films* **2007**, *515*, 3597.

[15] H. Liang, X. Geng, W. Li, A. Panepinto, D. Thiry, M. Chen, R. Snyders, *Coatings* **2019**, *9*, 361.

[16] D. Cossement, F. Renaux, D. Thiry, S. Ligot, R. Francq, R. Snyders, *Appl. Surf. Sci.* **2015**, *355*, 842.

[17] W. C. Oliver, G. M. Pharr, *J. Mater. Res.* **1992**, *7*, 1564.

[18] ISO145577-4, International Organization for Standardization 2007, 82, 24.

[19] D. Thiry, M. Pouyanne, D. Cossement, A. Hemberg, R. Snyders, *Langmuir* **2018**, *34*, 7655.

[20] C. Nouvellon, R. Belchi, L. Libralesso, O. Douhéret, R. Lazzaroni, R. Snyders, D. Thiry, *Thin Solid Films* **2017**, *630*, 79.

[21] S. Guimond, U. Schütz, B. Hanselmann, E. Körner, D. Hegemann, *Surf. Coat. Technol.* **2011**, *205*, S447.

[22] D. Thiry, N. Britun, S. Konstantinidis, J.-P. Dauchot, M. Guillaume, J. R. M. Cornil, R. Snyders, *J. Phys. Chem. C* **2013**, *117*, 9843.

[23] M. Witkowska, G. E. Thompson, T. Hashimoto, E. Koroleva, *Surf. Interface Anal.* **2013**, *45*, 1585.

[24] F. Mansfeld, *J. Appl. Electrochem.* **1995**, *25*, 187.

[25] F. Khelifa, S. Ershov, M.-E. Druart, Y. Habibi, D. Chicot, M.-G. Olivier, R. Snyders, P. Dubois, *J. Mater. Chem. A* **2015**, *3*, 15977.

[26] S. Ershov, M.-E. Druart, M. Poelman, D. Cossement, R. Snyders, M.-G. Olivier, *Corros. Sci.* **2013**, *75*, 158.

[27] N. Maître, T. Girardeau, S. Camelio, A. Barranco, D. Vouagner, E. Breelle, *Diamond Relat. Mater.* **2003**, *12*, 988.

[28] R. Förch, Z. Zhang, W. Knoll, *Plasma Processes Polym.* **2005**, *2*, 351.

[29] Q. Yu, H. Yasuda, *J. Polym. Sci., Part A: Polym. Chem.* **1999**, *37*, 1577.

[30] C. Lopez-Santos, J. L. Colaux, J. C. Gonzalez, S. Lucas, *J. Phys. Chem. C* **2012**, *116*, 12017.

[31] A. Von Keudell, M. Meier, C. Hopf, *Diamond Relat. Mater.* **2002**, *11*, 969.

[32] D. Thiry, A. De Vreese, F. Renaux, J. L. Colaux, S. Lucas, Y. Guinet, L. Paccou, E. Bousser, R. Snyders, *Plasma Processes Polym.* **2016**, *13*, 316.

[33] S. Ligot, E. Bousser, D. Cossement, J. Klemberg-Sapieha, P. Viville, P. Dubois, R. Snyders, *Plasma Processes Polym.* **2015**, *12*, 508.

[34] S. R. Peri, B. Habersberger, B. Akgun, H. Jiang, J. Enlow, T. J. Bunning, C. F. Majkrzak, M. D. Foster, *Polymer* **2010**, *51*, 4390.

[35] S.-M. Baek, T. Shirafuji, S.-P. Cho, N. Saito, O. Takai, *Jpn. J. Appl. Phys.* **2010**, *49*, 08JF10.

[36] F. J. Aparicio, D. Thiry, P. Laha, R. Snyders, *Plasma Processes Polym.* **2016**, *13*, 814.

[37] T. R. Gengenbach, Z. R. Vasic, R. C. Chatelier, H. J. Griesser, *J. Polym. Sci., Part A: Polym. Chem.* **1994**, *32*, 1399.

[38] D. Thiry, R. Francq, D. Cossement, M. Guillaume, J. Cornil, R. Snyders, *Plasma Processes Polym.* **2014**, *11*, 606.

[39] L. Denis, D. Thiry, D. Cossement, P. Gerbaux, F. Brusciotti, Van De Keere, V. Goossens, H. Terryn, M. Hecq, R. Snyders, *Prog. Org. Coat.* **2011**, *70*, 134.

[40] S. Saboohi, S. A. Al-Bataineh, H. Safizadeh Shirazi, A. Michelmore, J. D. Whittle, *Plasma Processes Polym.* **2017**, *14*, 1600054.

[41] D. Hegemann, In *Comprehensive Materials Processing*, Elsevier, Cameron **2014**, p. 201.

SUPPORTING INFORMATION

Additional supporting information may be found online in the Supporting Information section.